



Fault interaction for the Beni-Ilmane (east of Algeria) seismic sequence on May 2010

Hamoud Beldjoudi¹

Received: 19 May 2020 / Accepted: 2 September 2020 / Published online: 14 September 2020
© Saudi Society for Geosciences 2020

Abstract

This work is aimed at understanding the interaction between faults of three moderate events of the seismic sequence which occurred on May 2010 in the region of Beni-Ilmane which belongs to the Hodna-Biban domain (east of Algeria). This seismic sequence occurred on a complex faulted fold located in the Biban region in the southern part of the Tellian Atlas. The first shock occurred on May 14, 2010, at 12:29 GMT ($M_w = 5.5$) either on a dextral plane oriented [Strike, Dip, Rake: $254^\circ, 74^\circ, 175^\circ$] or on a sinistral plane oriented [Strike, Dip, Rake: $345, 85, 16$]. Based on the stress change modeling, the fault plane with [Strike, Dip, Rake: $254^\circ, 74^\circ, 175^\circ$] is the one played for the first shock and starting the seismic sequence. I have also shown that the plane of the second shock which occurred on May 16 at 06:52 GMT ($M_w = 5.1$) oriented [Strike, Dip, Rake: $250^\circ, 55^\circ, 120^\circ$] is loaded by the first shock (Coulomb stress changes = 0.19 bar). The third shock occurred on May 23 at 13:28 GMT ($M_w = 5.2$) with plane oriented [Strike, Dip, Rake: $12^\circ, 57^\circ, 12^\circ$] was loaded by the two previous shocks (Coulomb stress changes = 0.04 bar). I have correlated aftershocks occurred during this seismic sequence with Coulomb stress changes modeling taking into account the contribution of the regional stress tensor shows that the greatest number of aftershocks is located in positive areas of total Coulomb stress changes with a percentage that exceeds 65%. The best results are obtained for thrust optimal planes oriented NE-SW.

Keywords Coulomb stress change · Focal mechanism · Beni-Ilmane · Algeria · Regional stress

Introduction

The 2010 Beni-Ilmane seismic sequence occurred on a complex faulted fold in the Biban region in the southern part of the Tellian Atlas (Fig. 1a, b). The region is bounded to the south by the northern front of the Hodna basin and to the north by the Soummam River valley. The epicentral area of the Beni-Ilmane seismic sequence is located at the boundary of two distinct geological domains: the Alpine Mountains and the Tellian Sub-Bibanique nappe in the north and the pre-Atlas domain in the south (Yelles-Chaouche et al. 2014 ; Beldjoudi et al. 2016). The seismic sequence hits the Beni-Ilmane region between May 14 and 23, 2010. Three moderate

shocks and 1431 aftershocks were recorded and located until May 31 (Table 1). The first shock with a moment magnitude of 5.5 M_w and seismic moment of 1.8×10^{17} Nm (Fig. 1c) occurred either on a dextral plane oriented [Strike1, Dip1, Rake1: $254^\circ, 74^\circ, 175^\circ$] or on sinistral plane oriented [Strike2, Dip2, Rake2: $345, 85, 16$]. The second shock hit the region with a moment magnitude M_w of 5.1 and seismic moment 5.5×10^{16} Nm, occurred on a reverse fault oriented [Strike, Dip, Rake: $250^\circ, 55^\circ, 120^\circ$] and the third shock occurred on a left-lateral fault [Strike, Dip, Rake: $12^\circ, 57^\circ, 12^\circ$] with a moment magnitude M_w 5.2 and a seismic moment 7.4×10^{16} Nm (Beldjoudi et al. 2016). In this work, I will try to understand the interaction between these three moderate events which occurred on three neighboring unconnected faults. A seismotectonic model of the seismic sequence is presented in Fig. 1c. I shown in this study that the fault F_1 oriented NE-SW is the fault plane related to the first shock (Fig. 1c). Many studies concerning fault interactions and Coulomb stress changes modeling were conducted in the north of Algeria. Lin et al. (2011) studied the interaction of the fault of the Zemmouri-Boumerdes earthquake with two

This article is part of the Topical Collection on *Seismic Hazard and Risk in Africa*

✉ Hamoud Beldjoudi
hamoud.beldjoudi@craag.edu.dz

¹ Research Centre of Astronomy Astrophysics and Geophysics (CRAAG), Algiers, Algeria

Table 1 Source parameters of the main events

Event	Mainshocks	Seismic source(°) strike dip rake	Confidence index (CI %)	Moment magnitude (Mw)	Seismic moment (Nm)	Length (km)	Width (km)	Reverse slip (m)	Right lateral slip (m)	Total slip (m)
1	May 10, 1010	254° 74° 175°	74	5.5	2.4×10^{17}	6	4.5	0.021	0.237	0.24
2	May 16, 2010	250° 55° 120°	63	5.1	5.3×10^{16}	2.6	2.4	0.235	0.136	0.27
3	May 23, 2010	12° 57° 12°	62	5.2	7.4×10^{16}	3.8	3.47	0.036	-0.171	0.17

The fault dimensions and ruptures are obtained from empirical relationships among magnitude and rupture (Wells and Coppersmith 1994). The confidence index (CI %) describes the uniqueness and the quality of the focal mechanism obtained by waveform modeling in Beldjoudi et al. (2016) the (CI) varying between 0 and 100%. A value of (CI > 70%) indicates a well-constrained solution; a value of (CI > 60) represents an acceptable solution

seismogenic structures in the border of the Mitidja basin: the Sahel Anticline and the Blida Structure. At a regional scale, Kariche et al. (2017), tried to explain the relationship in term of Coulomb stress changes between the major events which occurred in the North of Algeria during two century. On a local scale, Dabouz and Beldjoudi (2019) studied the fault interaction following the Mont Chenoua earthquake (Ms 6.0) on nearby fault structures in the epicentral area.

Seismic sequence

The 2010 Beni-Ilmane seismic sequence consists of three main moderate magnitude earthquakes that ruptured strike-slip, reverse, and strike-slip faults in the Biban region (Beldjoudi et al. 2016; Yelles-Chaouche et al. 2014). The shallow sequence started on May 14 with Mw = 5.5. A second shock hit the region on May 16 with Mw = 5.1, and a third shock hit the region again on May 23 with Mw = 5.2. The three shocks are at a depth of 6 km (Beldjoudi et al. 2016). The largest events of the sequence are listed in Table 1. The aftershock sequence has been recorded by a dense temporary network between May 14 and 31 (Yelles-Chaouche et al. 2014). A total of 1403 events have been relocated with a horizontal error ERH ranging between 0.5 km and 1 km and a vertical error ERZ ranged between 0.5 km and 2 km. The duration magnitude Md ranged from 1.3 to 4.9. The epicenters are shallow and located between 0.3 and 11.08 km (Yelles-Chaouche et al. 2014). Relocated aftershocks drew two seismogenic volumes that are oriented NNE and EW (Fig. 1).

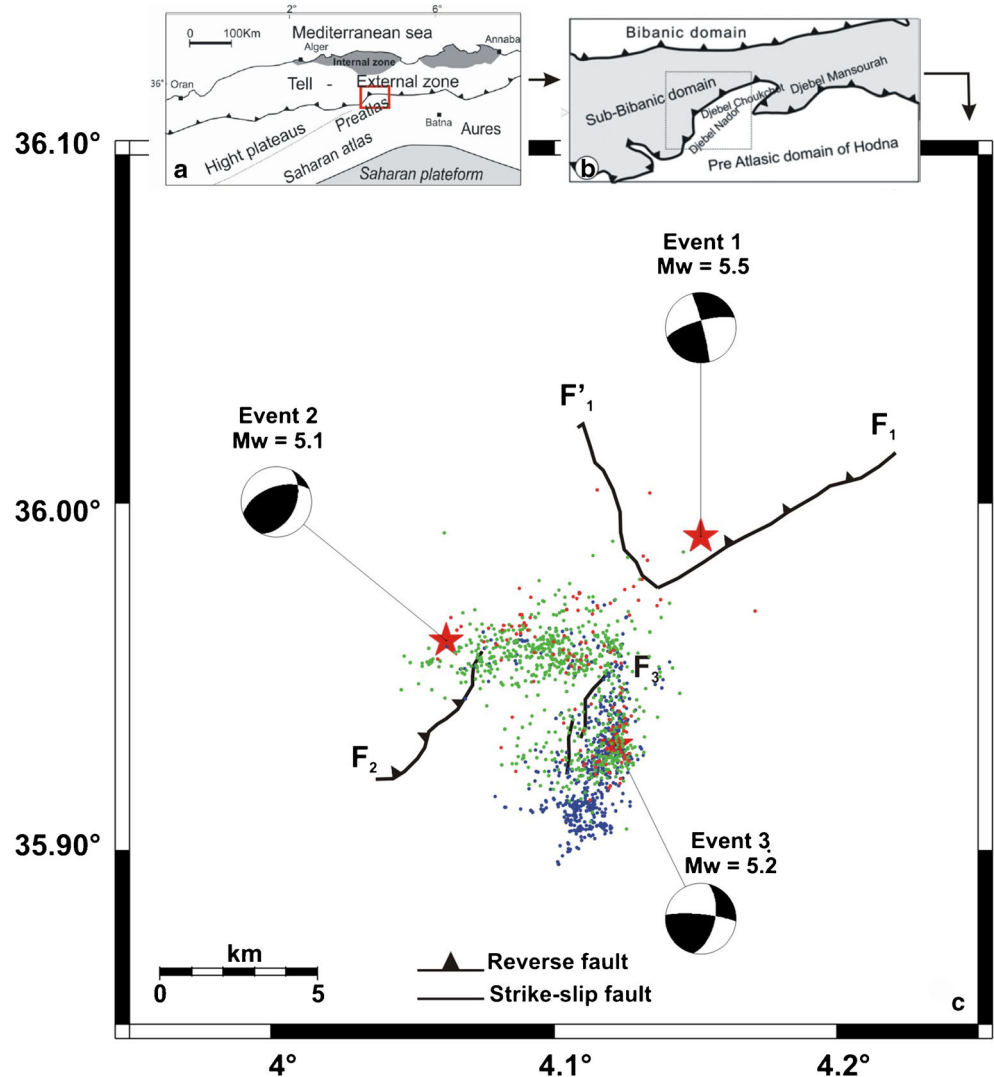
The aftershocks scenario can be divided into three episodes. The first episode started from the first shock (May 14, 12 h 29 min) until the occurrence of the second shock (May 16, 06 h 52 min); here, 118 events were relocated; the epicenters show diffuse seismicity with a semblance of orientation NE-SW; four shocks with a magnitude greater than 4 are located (Yelles-Chaouche et al. 2014). During the second period which started from the second shock until the third

shock (May 23, 13 h 28 min), two main clusters can be shown. One cluster oriented E-W located North of the second shock and extent ~ 12 km. The other cluster located SE of the second shock. During the third period (May 23 to 31), 591 events were relocated. In this period two main clusters were well identified: one oriented E-W and the other oriented NNE-SSW. Focal mechanisms of the mainshocks obtained by waveform modeling (Beldjoudi et al. 2016) show a strike-slip regime for the first shock, a reverse fault for the second shock, and a strike-slip for the third shock (Fig. 1). The spatial distribution of the main epicenters and spatio-temporal distribution of the aftershocks point out several peculiarities. First, the seismic sequence occurred in a faulted fold with faults oriented in all directions. Second, the three main shocks are located on unconnected faults of the fold with different FM. Third, the aftershocks are oriented in two orthogonal directions: NNE-SSW and E-W.

Seismicity of the Beni-Ilmane region

The Beni-Ilmane region belongs to the Hodna-Biban area. The seismicity of the region dates to the Zemmoura-Guenzet earthquake on February 9, 1850, with a maximum observed intensity (Io) of VII (European Macroseismic Scale, EMS) assigned by Harbi and Maouche (2009). Other earthquakes occurred in the region for the period (1850–1973), their intensity were greater than VII near the following localities: (1) M'sila on 1885 and 1965 (Harbi et al. 2003; Hatzfeld 1978; Rothé 1950); (2) Mansourah on 1887, 1943, and 1973 (Harbi et al. 2003; Hatzfeld 1978; Rothé 1950); (3) Berhoum on 1946; (4) Beni-Ilmane (formerly Melouza) on 1960; and (5) M'sila on 1885 and 1965 (Fig. 2). During the instrumental era, the Mansourah region has recorded the largest earthquake with magnitude of up to 4.9 during the period 1973–1974; also on May 5, 2012, an earthquake of Mw 4.9 hit the region of Bordj Bou Arreridj (northeast of Mansourah). Historical and instrumental catalogs (Mokrane et al. 1994, Harbi and

Fig. 1 **a** Location of the epicentral area at a regional scale, **b** location of the epicentral area at a local scale, and **c** seismotectonic map of the epicentral area. Stars show the location of the main events and their relative focal mechanisms. Red dots are aftershocks for the first period (May 14–16), green dots are aftershocks for the second period (May 16–23), and blue dots are aftershocks for the third period (May 23–31). F_1 , F_1' , and F_2 are the identified faults close to the location of the main event



Mauouche 2009) show that the Hodna-Biban region is seismically active; the seismicity is distributed on numerous active structures. The maximum observed intensity (I_0) values of VIII–IX have been observed in the area of Mansourah (Roussel 1973; Bezzeghoud et al. 1996; Boughacha et al. 2004).

Coulomb stress changes

I calculate Coulomb stress changes (ΔCFF) using the Coulomb 3.3 software (Toda et al. 2005a, b; Lin and Stein 2004). The static stress changes caused by an earthquake are computed using the Coulomb failure assumptions (King et al. 1994; Hodgkinson et al. 1996; Harris 1998; Cocco et al. 2000). The variation of the Coulomb stress changes (ΔCFF) is defined as (Stein et al. 1992; Harris 1998)

$$\Delta CFF = \Delta\tau + \mu (\Delta\sigma + \Delta P) \tag{1}$$

where $\Delta\tau$ is the change in shear stress, $\Delta\sigma$ is the change in normal stress (positive for extension), μ is the friction coefficient, and ΔP is the change in pore pressure. This latter term can be expressed in terms of the Skempton’s coefficient B as follows (Harris 1998; Cocco et al. 2000):

$$\Delta P = -B \frac{\Delta\sigma_{kk}}{3} \tag{2}$$

where $\Delta\sigma_{kk}$ is the volumetric stress change and σ_{kk} is the sum of the normal stresses ($\sigma_{kk} = \sigma_{11} + \sigma_{33}$).

The Skempton’s coefficient can vary between 0 and 1 (Roeloffs 1988; Cocco et al. 2000). Commonly, it is assumed that the fault zone materials are more ductile than the surrounding materials (Rice 1992; Harris 1998). Under these conditions, $\frac{\Delta\sigma_{kk}}{3} \sim \Delta\sigma_n$, and Eq. (1) is frequently written as

$$\Delta CFF = \Delta\tau + \mu' \Delta\sigma_n \tag{3}$$

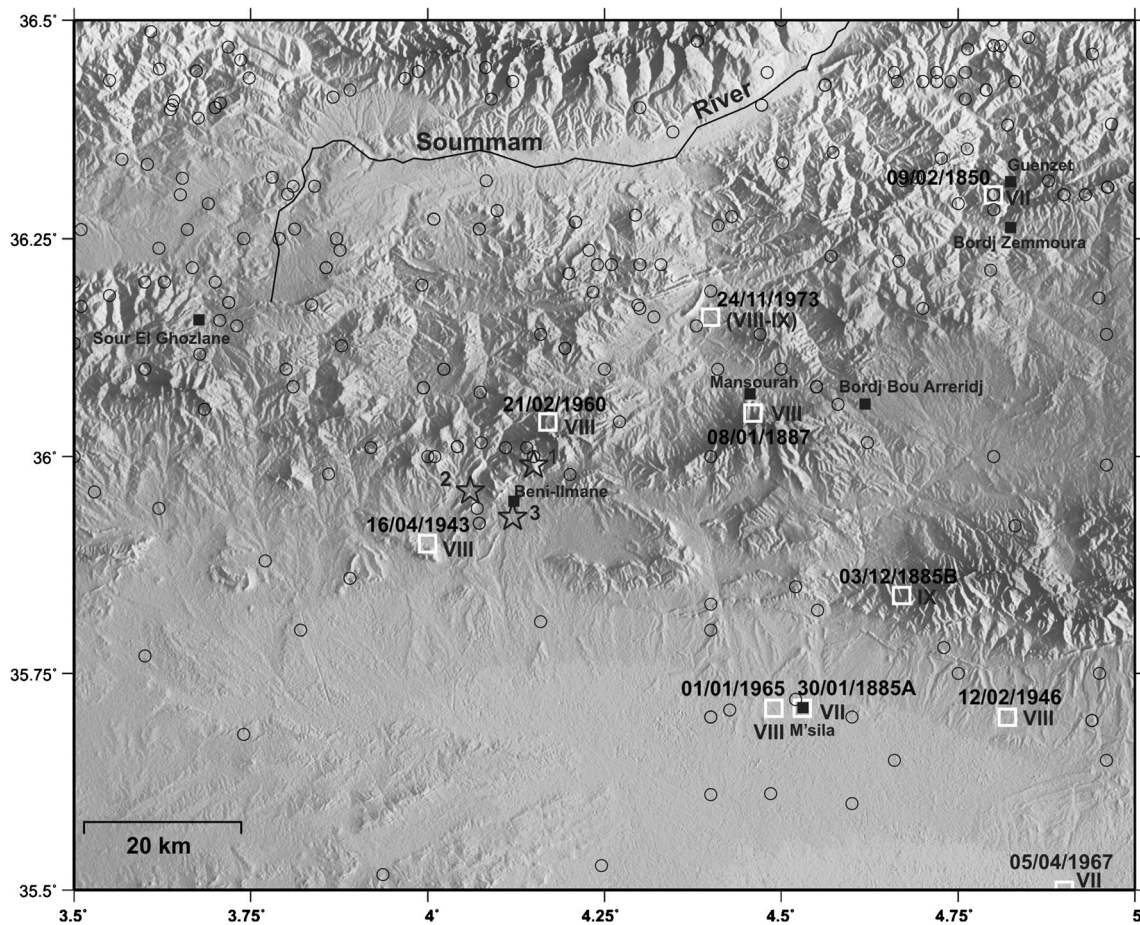


Fig. 2 Historical seismicity in the Hodna-Biban region from February 9, 1850, to May 13, 2010. White open squares show the main earthquakes (historical) reported in the region. Open circles show instrumental

seismicity. Open stars show the main events of the seismic sequence. Black solid squares indicate cities and villages in the region

where $\Delta\tau$ is the change in shear stress, $\Delta\sigma$ is the change in normal stress, $\mu' = \mu(1 - B)$ is the effective friction coefficient, and μ is the coefficient of friction. Many studies suggest that μ is (0.6–0.9) for most geological materials and the effective friction coefficient μ' used in triggered seismicity is defined by the combination of pore pressure and friction coefficient (Byerlee 1978; Kariche et al. 2017). Previous studies suggest that one explanation for apparently low value of μ' would be the presence of high fluid pressure (Kariche et al. 2017, Jaumé and Sykes 1992). In our study, I show that the coulomb modeling requires an effective friction coefficient of $0.1 < \mu' < 0.8$ which implies a ΔCFF of 0.18 bar at the hypocenter of the receive fault2. Equation (3) is commonly used to calculate Coulomb stress changes by assuming different values for μ' where the influence of pore pressure is included in the effective coefficient of friction (Fig. 3).

Regional stress

The Coulomb stress modeling on optimally oriented fault planes are computed by considering both, the static

stress changes σ_{ij}^c and the regional tectonic stress σ_{ij}^r (King et al. 1994)

$$\sigma_{ij}^t = \sigma_{ij}^r + \sigma_{ij}^c \tag{4}$$

In this case, the ΔCFF is computed using the total stress tensor σ_{ij}^t , as shown by Eq. (4).

Many studies were conducted to calculate regional stress in many regions in North of Algeria; the general trend of the regional stress is NW-SE (Khelif et al. 2018; Soumaya et al. 2018; Beldjoudi et al. 2009, 2012, 2016). The regional stress was obtained for the region of the Beni-Ilmane by inversion of strike and dip of the focal mechanisms available in the region (Beldjoudi et al. 2016). The principal-compressive stress axis σ_1 is oriented N160° and plunged 22°, the intermediate stress σ_2 oriented N20° and plunged 62° and the extensive stress σ_3 , is oriented N77° and plunged 16°. The trend of regional stress is used in this study to calculate Coulomb stress changes on optimal planes.

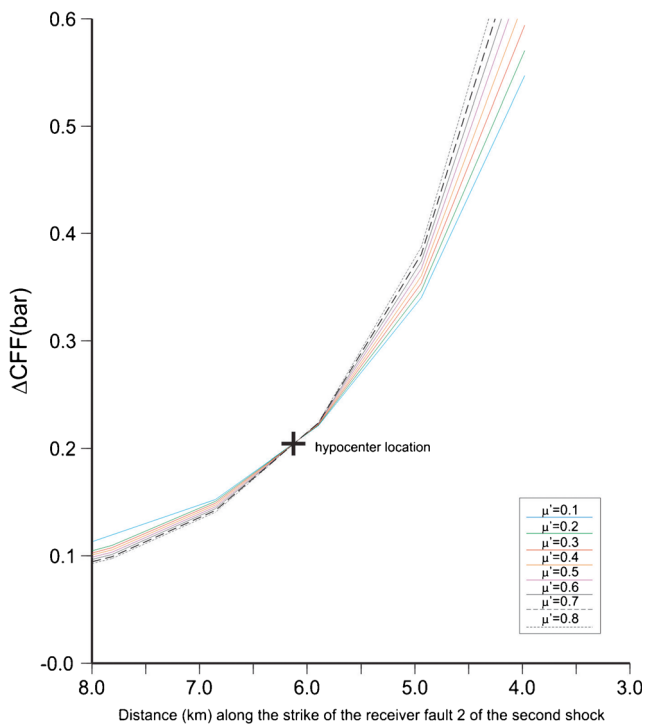


Fig. 3 Stress loading the receiver fault 2 ($256^{\circ}/55^{\circ}/120^{\circ}$) with a source fault oriented ($254^{\circ}/74^{\circ}/175^{\circ}$) using different effective friction coefficient μ' . Black cross shows epicenter location

Coulomb stress changes following the first shock and the second shock

On 14 May 2010 starts the seismic sequence of the Beni-Ilmane region with a first shock of Mw 5.5. The focal mechanism calculated by waveform inversion (Beldjoudi et al. 2016) shows a right lateral strike-slip fault with an azimuth of $N254^{\circ}$ for the first plane and a left lateral $N345^{\circ}$ for the second plane. The question is: Which fault plane of the focal mechanism played during this first shock? In the previous studies (Beldjoudi et al. 2016; Yelles-Chaouche et al. 2014), no one could answer this question, because the epicenter is located near two active structures and no surface trace was visible because the shock is moderate. For this, I will consider both planes as sources, and I will compute the Coulomb stress changes (ΔCFF) on considering receiver faults, the second and third shocks, and then I will compare the results.

I start to calculate (ΔCFF) considering first the plane oriented $N345^{\circ}$ as a seismic source. The receiver faults of the second and the third shocks were identified (Beldjoudi et al. 2016; Yelles-Chaouche et al. 2014) and are oriented $N250^{\circ}$ and $N12^{\circ}$, respectively. I calculated the (ΔCFF) at a depth of 6 km and will assume the effective coefficient of friction $\mu' = 0.4$ for all modeling procedure.

Fig. 4a, b show that the seismic source of the plane oriented (Strike, Dip, Rake: 345° , 85° , 16°) load the receiver fault oriented $N250^{\circ}$ of the second shock and the calculated

(ΔCFF) is positively equal 0.07 bar but may not be enough to trigger the second shock (less than threshold value of 0.1 bar).

Figure 4c and d show the calculated (ΔCFF) with the contribution of the plane oriented (Strike, Dip, Rake: 345° , 85° , 16°) of the first shock and the plane oriented (Strike, Dip, Rake: 250° , 55° , 120°) of the second shock as sources. The receiver fault corresponds to the plane oriented (Strike, Dip, Rake: 12° , 57° , 12°) which corresponds to the third shock. The computed (ΔCFF) shows that this plane is located in the area where the $9(\Delta CFF)$ is negative. This means that the third shock cannot be promoted by the previous shocks because the value of (ΔCFF) is negative (-0.49 bar).

Then, I calculate (ΔCFF) considering a seismic source for the second plane of the first shock oriented (Strike, Dip, and Rake: 254° , 74° , 175°) and the receiver fault as the second shock oriented $N250^{\circ}$. This fault is located in a positive area of ΔCFF with a value of 0.18 bar, enough to promote the second shock (Fig. 5a,b), and also I compute the (ΔCFF), considering as source the plane oriented $N254^{\circ}$ and the plane oriented $N250^{\circ}$ (Fig. 5c,d). The receiver fault is the third shock oriented (Strike, Dip, Rake: 12° , 57° , 12°). The fault is located in an area with positive (ΔCFF) and has a value of 0.04 bar. This is less than the threshold value (Stein et al. 1992), but if I compare it to the first case, I will assume that the plane oriented $N254^{\circ}$ is the fault plane that played during the first shock.

Correlating the aftershock distribution with the static stress changes

In this section, I will correlate the aftershock distribution with the Coulomb stress changes obtained from the contribution of the static stress changes and the regional tectonic stress (Stein et al. 1992; King et al. 1994; Nostro et al. 1997) in the aim to find the optimally oriented planes (see section above). In the following, I will call this contribution the total Coulomb stress changes (ΔCFF).

I have considered three-time windows that represent the number of periods of the seismic sequence (Fig. 6a). The first period goes from 14 to 16 May at 06:52 UTM. The second period goes from 16 May at 06:52 UTM to 23 May at 13:28 UTM and the last period is from 23 May at 13:28 UTM to 31 May at 22:46 UTM. The catalog used in this study is from Yelles-Chaouche et al. (2014).

Coulomb stress changes and aftershock distribution for period 1 (May 14–16)

In this session, I computed total Coulomb stress changes σ'_{ij} taking into account the contribution of the static stress changes

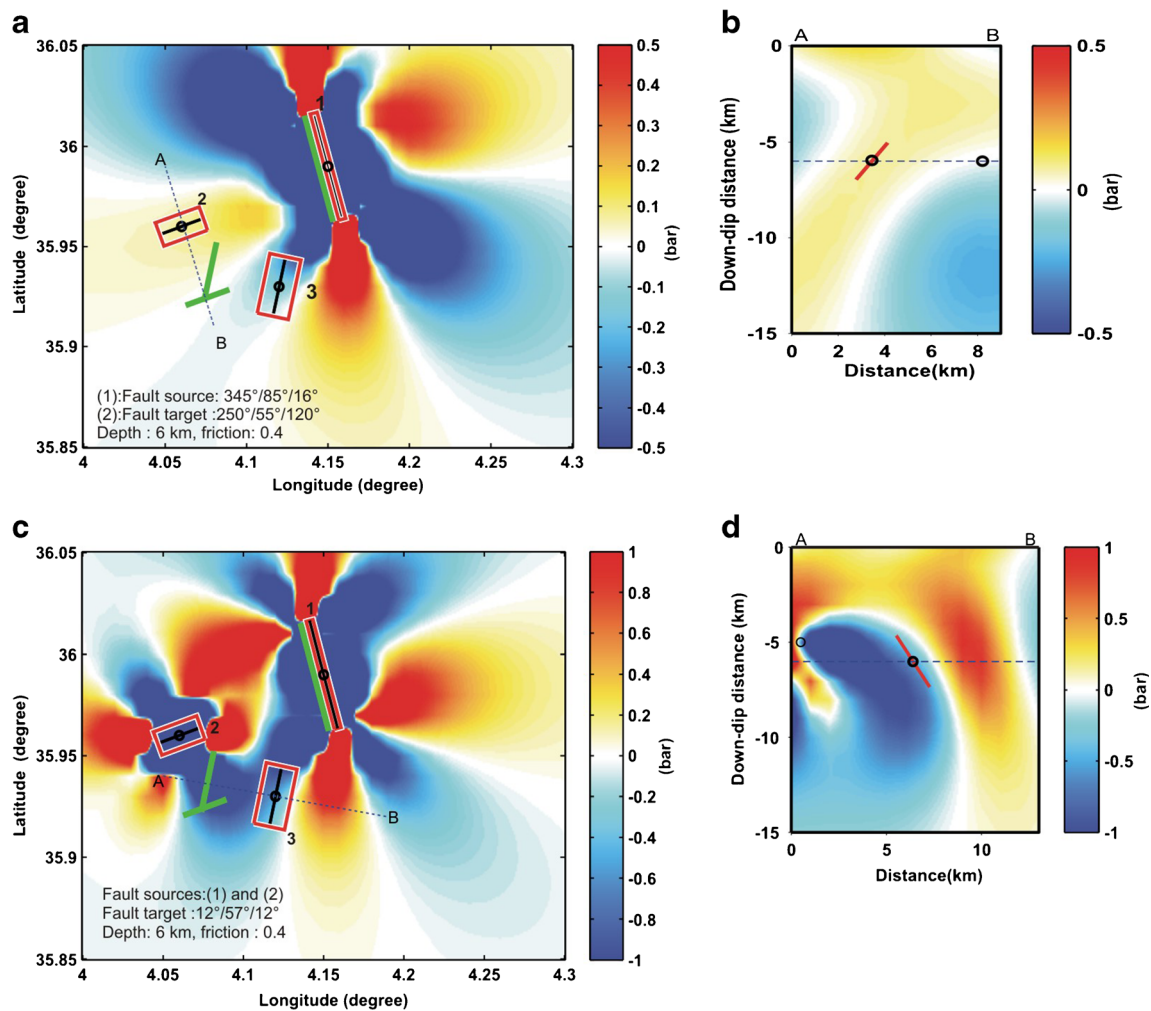


Fig. 4 **a** Coulomb stress change (ΔCFF) associated with the plane of the first shock ($345^\circ/85^\circ/16^\circ$) resolved on the plane of the second shock oriented ($250^\circ/55^\circ/120^\circ$) at a depth of 6 km. (1), (2), and (3) are the faults of the seismic sequence. **b** Cross-section shows the variation of the (ΔCFF) with depth, **c** (ΔCFF) associated with the first and second shocks ($345^\circ/85^\circ/16^\circ$) and ($250^\circ/55^\circ/120^\circ$) resolved on fault plane ($12^\circ/57^\circ/120^\circ$) of the third shock, and **d** cross-section shows the variation of the (ΔCFF) with depth. Fault 3 is located in an area where ($\Delta CFF < 0$). Coefficient of friction ($\mu' = 0.4$). For all figures, the green lines are the fault trace projected up-dip. Red lines are the edge of the fault projected vertically to surface. Black line is the intersection of the target depth with the fault plane

σ_{ij}^c and the regional stress σ_{ij}^r on strike-slip optimal planes and thrust optimal planes for the period 1 from May 14 to 16 (06 h 52 min) (occurrence of the second shock). Aftershocks in this period show two main directions, an \sim EW and a \sim NNE-SSW; the depths of aftershocks are between 1.3 and 9.78 km.

I have computed (ΔCFF) on strike-slip optimal planes and on thrust optimal planes for this period. The best correlation is obtained for thrust optimal planes. I computed the (ΔCFF) between 2 and 9 km with a step of 1 km, and for each step, I plotted aftershocks located in the range of depth ± 0.5 km for optimal thrust planes oriented NE-SW. For some 117 plotted aftershocks, I obtained 21% of them located in an area with a negative Coulomb stress changes, and 79% were located in a positive area. In Fig. 6b, I presented (ΔCFF) computed for thrust optimal planes for a depth of 6 km. I plotted aftershocks located between 5.51 and 6.5 km. The results showed that 28

aftershocks are in the area of positive stress and only three of them are in a negative area. Generally, the results are the same for the other depth- (ΔCFF) correlation, and the number of aftershocks located in a positive area is the most important. The cross-section in Fig. 6c confirms also these results.

Coulomb stress change and aftershock distribution for period 2 (May 16 to 23)

In this section, I computed the (ΔCFF) for thrust optimal planes and plotted the aftershocks that occurred during period 2 (May 16 to 23). A total of 695 aftershocks were located with a depth of 0.3 to 11.08 km. Two clusters are visible with EW and NNE-SSW trends (Fig. 1). For the total number of aftershocks for this period, I located 17% of them in the negative area and 83% in the positive area of Coulomb stress changes.

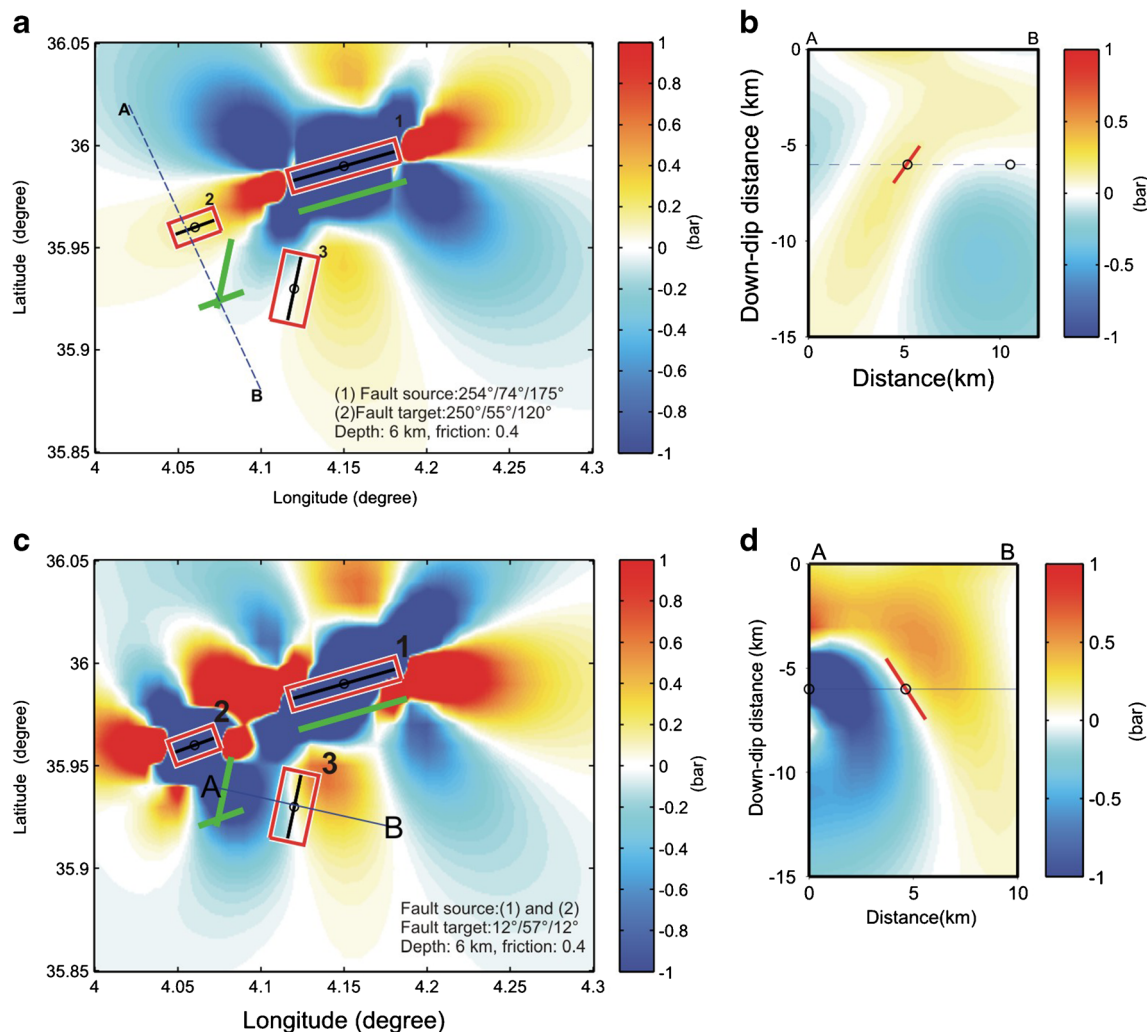


Fig. 5 **a** (Δ CFF) associated with the plane of the first shock ($254^\circ/74^\circ/175^\circ$) resolved on the plane of the second shock oriented ($250^\circ, 55^\circ, 120^\circ$) at a depth of 6 km. **b** Same as Fig. 2b. **c** (Δ CFF) associated with

the first and second shocks ($254^\circ/74^\circ/175^\circ$) and ($250^\circ/55^\circ/120^\circ$) resolved on fault plane ($12^\circ/57^\circ/120^\circ$) of the third shock. **d** Same as Fig. 2d

In Fig. 7a and b, I presented (Δ CFF) computed for thrust optimal planes at a depth of 6 km oriented NE-SW. The plotted aftershocks are located between 5.51 and 6.5 km of depth and present a good correlation with Coulomb stress changes load.

Coulomb stress change and aftershock distribution for the period 3 (May 23 to 31)

In this part, I computed (Δ CFF) caused by the contribution of the three major events of the seismic sequence and the regional stress on thrust and strike-slip optimal planes. A number of 590 aftershocks were located for this period (May 23 to 31 at 22 h 46 min); the depths are between 1.22 and 9.72 km with a duration magnitude M_d of 1.3 to 4.9. Two clusters are visible with EW and NNE-SSW trends (Fig. 1). First, distribution of aftershocks was correlated with (Δ CFF) computed for thrust optimal faults; the results are 60% located on the negative

area, and only 40% are located on the positive area. In Fig. 8a and b, I computed (Δ CFF) at a depth of 6 km and plotted aftershocks located between 5.51 and 6.5 km for this third period. It was confirmed that the major aftershocks were located in the negative area. Also, (Δ CFF) were computed for strike-slip optimal planes, and the results of the correlation are less good than obtained for optimal thrust planes.

Conclusion

The main goal of our study is the investigation of fault interaction through elastic stress transfer among the subsequent moderate size earthquakes that occurred during the 2010 seismic sequence of the Hodna basin in the transitional zone of the sub-Bibanic and the pre-Atlasic domain (Fig. 1). I investigate the spatial distribution of aftershocks, and I try to explain it in terms of Coulomb stress changes caused by a sequence of

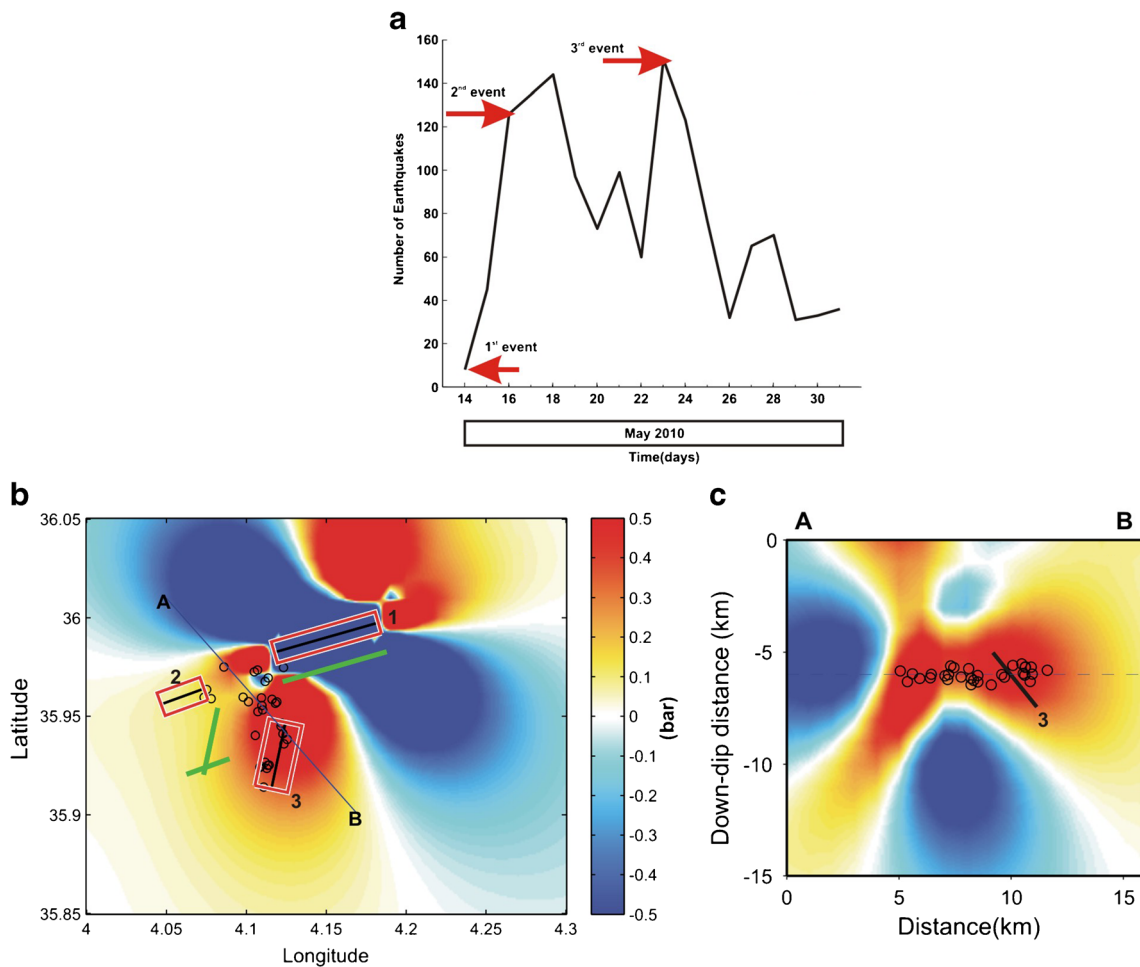


Fig. 6 **a** Plot of the number of earthquakes versus time. The red arrows indicate the occurrence of the main events. **b** Map showing the Coulomb changes computed from the contribution of the (ΔCFF) of the fault 1, and the regional tectonic stress at 6 km of depth resolved on optimal thrust

faults (NE-SW). Aftershocks located during the period 1 plotted between 5.51 km and 6.50 km (± 0.5 km) of depth. **c** Cross-section showing the location of the same aftershocks. Black line is the fault 3

subsequent mainshocks. As presented in the previous session, the seismic sequence was divided into three periods. The period 1 started from the first shock until the occurrence of the

second shock (14-16 May). The period 2 is from the second shock until the occurrence of the third shock that concern only the interaction between the main events. To correlate the

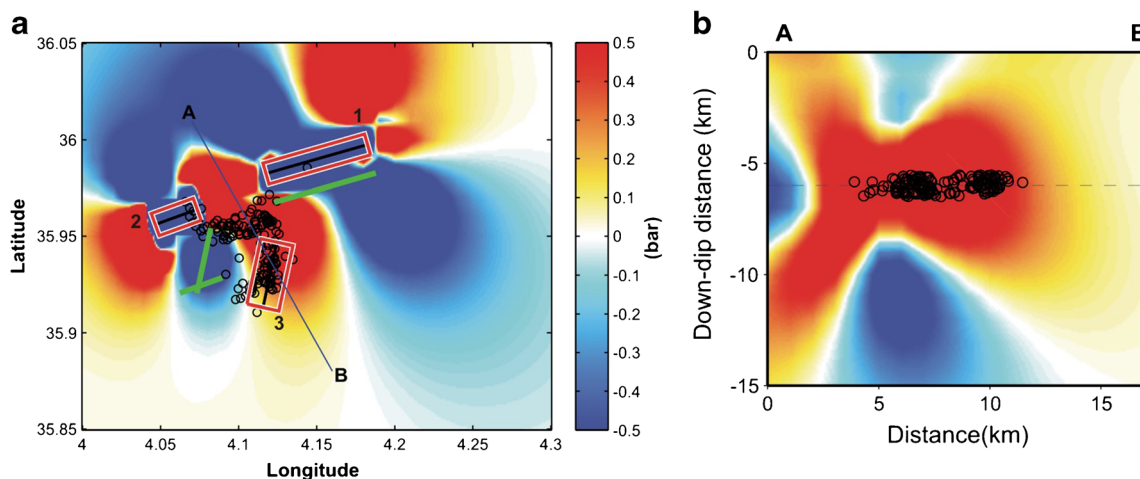


Fig. 7 Same as Fig. 6 but for period 2

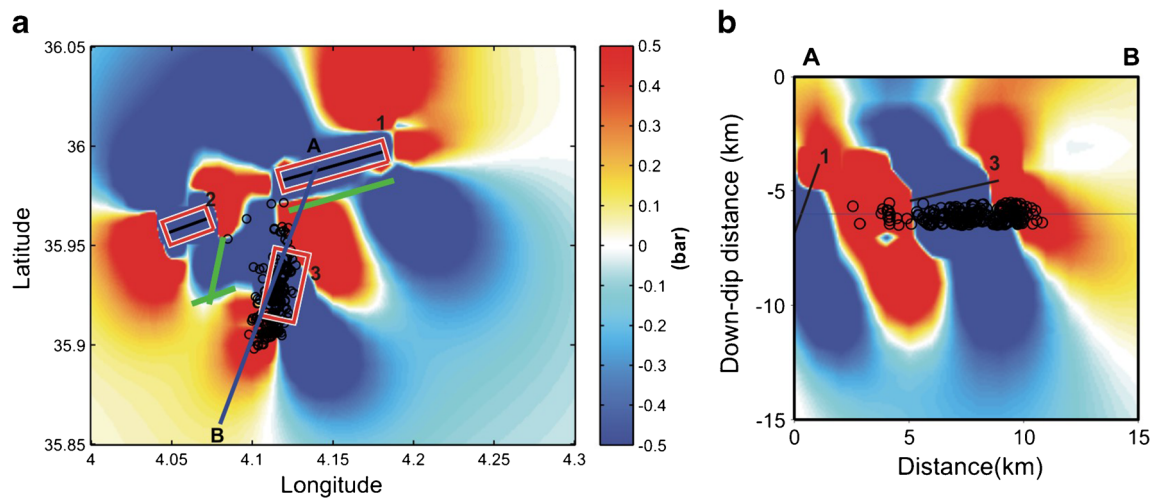


Fig. 8 Same as Fig. 6 but for period 3

distribution of aftershocks with Coulomb stress changes, I have added a period 3 which starts from the third event and stopped on 31 May of last located aftershock in the catalog of Yelles-Chaouche et al. (2014).

The results presented in this paper shows that Coulomb stress changes correlate well with the position, geometry, and slip direction of these segments. I concluded also that Coulomb interaction exists and each mainshock promoted the rupture of the following event. I identified the fault plane that played during the first shock by comparing the amount of the (ΔCFF) produced by each plane of the focal mechanism of the first event. I have shown also that the fault plane oriented $N254^{\circ}/75^{\circ}/175^{\circ}$ is the one that ruptured during the first event. This plane ($254^{\circ}/75^{\circ}/175^{\circ}$) promoted the rupture of the plane ($250^{\circ}/55^{\circ}/120^{\circ}$) of the second shock. The contribution of these two first events promoted the occurrence of the third event ($12^{\circ}/57^{\circ}/12^{\circ}$).

On the other hand, I have tried to explain the distribution of the aftershocks with the variation of the Coulomb stress. In this work, I have shown that the aftershocks correlated well with the (ΔCFF) when this is calculated on optimal thrust faults. In period 1, 79% of aftershocks (total of 117) were located in the area of positive (ΔCFF), while 21% of them were in the negative area. In period 2, 83% of aftershocks (total of 695) are in the positive area, while 17% are located in the negative area. In period 3, out of 590 aftershocks, only 40% are located in the positive area and 60% in the negative area which is contrary to our observation in the two previous periods. I computed then (ΔCFF) on strike-slip optimal faults; the results obtained were less good than those obtained for thrust optimal planes; I found only 20% of aftershocks located in the positive area, and the rest are located in the negative area. This study shows that despite the fact that the faults appear unconnected, the change in the stress state around the faulted fold during the seismic sequence made them connected in terms of Coulomb stress changes, and each one played

under the effect of the preceded shock. This study also reinforced the number of studies conducted in the region based on its seismic source, seismotectonic, and fault interaction.

Acknowledgments I am grateful to Prof. Mustapha Meghraoui (University of Strasbourg, France) for reading an early version of the article and for his valuable comments. I also thank anonymous reviewers for their valuable comments and suggestions for improving the article. I thank Prof. Yelles-Chaouche Abdelkrim for providing me the aftershocks catalog of the seismic sequence.

Funding This study is supported by the Centre de Recherche en Astronomie Astrophysique et Géophysique (CRAAG, Ministry of Interior) and the Seismology Division.

References

- Beldjoudi H, Delouis B, Djellit H, Yelles-Chaouche A, Gharbi S, Abacha I (2016) The Beni-Ilmane (Algeria) seismic sequence of May 2010: seismic sources and stress tensor calculations. *Tectonophysics* 670: 101–114. <https://doi.org/10.1016/j.tecto.2015.12.021>
- Beldjoudi H, Delouis B, Heddar A, Nouar OB, Yelles-Chaouche A (2012) The Tadjena earthquake (Mw = 5.0) of December 16, 2006 in the Cheliff region (Northern Algeria): waveform modelling, Regional stresses, and relation with the Boukadir fault. *Pure Appl Geophys* 169:677–691
- Beldjoudi H, Guemache MA, Kherroubi A, Semmane F, Yelles-Chaouche A, Djellit H, Amrani A, Haned A (2009) The Lâalam (Béjaïa North–East Algeria) moderate earthquake (Mw = 5.2) on March 20, 2006. *Pure Appl Geophys*. <https://doi.org/10.1007/s00024-009-0462-9>
- Bezzeghoud M, Ayadi A, Sebai A, Ait Messaoud A, Mokrane A, Benhallou H (1996) Seismicity of Algeria between 1365 and 1989: map of maximum observed intensities(MOI), *Avances en Geophysica y Geodesia* 1, año 1. Ministerio de Obras Publicas, Transportes y Medio Ambiente, Instituto Geographico Nacional España, pp. 107–114.
- Boughacha MS, Ouyed M, Ayadi A, Benhallou H (2004) Seismicity and seismic hazard mapping of northern Algeria: map of maximum calculated intensities. *J Seismol* 8:1–10

- Byerlee J (1978) Friction of rocks. *Pure Appl Geophys* 116(4/5): 615–626
- Cocco M, Nostro C, Ekström G (2000) Static stress changes and fault interaction during the 1997 Umbria-Marche earthquake sequence. *J Seismol* 4:501–516
- Dabouz G, Beldjoudi H (2019) Interaction Faults in the North-West of the Mitidja Basin: Chenoua–Tipasa–Ain Benian Earthquakes (1989–1996), Part of the *Advances in Science, Technology & Innovation* book series (ASTI), https://doi.org/10.1007/978-3-030-01656-2_59
- Harbi A, Maouche S (2009) Les principaux séismes du Nord-Est de l'Algérie Mémoires du Service Géologique National, No 16
- Harbi A, Maouche S, Benhallou H (2003) Re-appraisal of seismicity and seismotectonics in the north-eastern Algeria II: 20th century seismicity and seismotectonic analysis. *J Seismol* 7:221–234
- Hatzfeld D (1978) Etude sismotectonique de la zone de collision Ibéro-Maghrébine Thèse de doctorat ès-Sciences Physiques Laboratoire de Géodynamique Interne, Université Scientifique et Médicale de Grenoble, p. 281.
- Harris RA (1998) Introduction to the special section: stress triggers, stress shadows, and implication for seismic hazard. *J Geophys Res* 10: 24347–24358
- Hodgkinson KM, Stein RS, King GCP (1996) The 1954 Rainbow Mountain-Fairview Peak-Dixie Valley earthquakes: a triggered normal faulting sequence. *J Geophys Res* 101:25,459–25,471
- Jaumé SC, Sykes LR (1992) Changes in state of stress on the Southern San Andreas fault resulting from the California earthquake sequence of April to June 1992. *Science* 258:1325–1328
- Kariche J, Meghraoui M, Ayadi A, Boughacha MS (2017) Stress change and fault interaction from two century-long earthquake sequence in the central Tell Atlas, Algeria. *Bull Seismol Soc Am*. <https://doi.org/10.1785/0120170041>
- Khelif M, Yelles-Chaouche A, Benaissa Z, Semmane F, Beldjoudi H, Haned A, Issaadi A, Chami A, Chimouni R, Harbi A, Maouche S, Dabbouz G, Aidi C, Kherroubi A (2018) The 2016 Mihoub (north-central Algeria) earthquake sequence: seismological and tectonic aspects. *Tectonophysics* (2018) 736:62–74. <https://doi.org/10.1016/j.tecto.2018.03.015>
- King GCP, Stein RS, Lin J (1994) Static stress changes and the triggering of earthquakes. *BSSA* 84(3):935–953
- Lin J, Stein RS, Meghraoui M, Toda S, Ayadi A, Dorbath C, Belabbes S (2011) Stress transfer among en echelon and opposing thrusts and tear faults: triggering caused by the 2003 Mw = 6.9 Zemmouri, Algeria, Earthquake. *J Geophys Res* 116:B03305. <https://doi.org/10.1029/2010JB007654>
- Lin J, Stein RS (2004) Stress triggering in thrust and subduction earthquakes and stress interaction between the southern San Andreas and nearby thrust and strike-slip faults. *J Geophys Res* 109(B02303): 2004. <https://doi.org/10.1029/2003JB002607>
- Mokrane A, Aït Messaoud A, Sebaï A, Menia A, Ayadi A, Bezzeghoud M (1994) Les séismes en algérie de 1365 à 1992. Publication du Centre de Recherche en Astronomie Astrophysique et Géophysique. Supervised by Bezzeghoud M. and Benhallou H. Alger-Bouzaréah p. 277
- Nostro C, Cocco M, Belardinelli ME (1997) Static stress changes in extensional regimes: An application to the Southern Apennines (Italy). *Bull Seismol Soc Am* 87:234–248
- Roeloffs LA (1988) Fault stability changes induced beneath a reservoir with cyclic variations in water level. *J Geophys Res* 93:2107–2124
- Rice JR (1992) Fault stress states, pore pressure distributions, and the weakness of the San Andreas fault. In: Evans B, Wong T-F (eds) *Fault Mechanics and Transport Properties of Rock*. A Festschrift in Honor of W. F. Brace. Academic, San Diego, pp 475–503
- Rothé JP (1950) Les séismes de Kherrata et la sismicité de l'Algérie. *Bull. ser. Carte géologique de l'Algérie*, 4e série, Géophysique n° 3.
- Roussel J (1973) Les zones actives et la fréquence des séismes en Algérie 1716–1970. *Bull Soc Hist Nat Afr Nord* 64(3):211–227
- Soumaya A, Ben Ayed N, Rajabi M, Meghraoui M, Delvaux D, Kadri A, Ziegler M, Maouche S, Braham A (2018) Active faulting geometry and stress pattern near complex strike-slip systems along the Maghreb region: constraints on active convergence in the Western Mediterranean. *Tecton Am Geophys Union (AGU)* 37(9):3148–3173. <https://doi.org/10.1029/2018TC004983>
- Stein RS, King GCP, Lin J (1992) Change in failure stress on the southern San Andreas fault system caused by the 1992 magnitude =7.4 Landers earthquake. *Science*. 258:1328 1992
- Toda S, Stein RS, Richards-Dinger K, Bozkurt S (2005a) Forecasting the evolution of seismicity in southern California: animations built on earthquake stress transfer. *J Geophys Res* 110:B05S16. <https://doi.org/10.1029/2004JB003415>
- Toda S, Stein RS, Reasenber PA, Dietrich JH, Yoshida A (2005b) Stress transferred by the 1995 Mw = 6.9 Kobe, Japan, Shock: effects on aftershocks and future earthquake probabilities. *J Geophys Res* 103: 24543–24566
- Wells DL, Coppersmith KJ (1994) New empirical relationships among magnitude, rupture length, rupture width, rupture area, and surface displacement. *Bull Seis Soc Am* 84(4):974–1002
- Yelles-Chaouche A, Abacha I, Semmane F, Beldjoudi H (2014) The Beni-Ilmane (north-central Algeria) earthquake sequence of May 2010. *Pure Appl Geophys*. <https://doi.org/10.1007/s00024-013-0709-3>